In-plane mechanical properties of a novel hybrid auxetic structure

Peng Fan[1,3], Yu Chen[1], Jian Xiong[2] and Hong Hu[1,a]

[1]*Institute of Textile and Clothing, The Hong Kong Polytechnic University, Hong Kong, China*

[2]*Center for Composite Materials and Structures, Harbin Institute of Technology Harbin, China*

[3] *School of Mechanical Engineering, Xi'an Jiaotong University, Xi'an, China*

(a) Corresponding author. Email: hu.hong@polyu.edu.hk

Abstract

This paper presents a novel hybrid auxetic structure with the enhanced mechanical properties by combining the re-entrant and double-arrowhead structures based on the structural stretching-dominated deformation mechanism. The unit cell of the developed hybrid structure is comprised of an external quadrilateral frame and an internal arrowhead part. The theoretical analysis model for predicting its in-plane mechanical properties in the two principal directions is presented and verified by both numerical simulations and experimental measurements. On this basis, a parametric study on the in-plane mechanical performance of the hybrid structure is performed to optimize geometrical parameters. The results show that both the negative Poisson's ratio behavior and the mechanical performance of the hybrid structure can be enhanced by increasing the length of the vertical wall or reducing the angle of the inclined wall in the internal arrowhead part. The hybrid structure with the obvious difference of the mechanical properties between the two principle directions can be obtained by individually adjusting the width of the hybrid unit cell, while the mechanical performance in both two directions can be improved by simultaneously reducing the length of the vertical wall and the width of the hybrid unit cell. In addition, compared with the re-entrant structure, the hybrid structure demonstrates higher elastic moduli and a wider range of Poisson's ratio from negative to positive. The study provides a guidance for the optimized design of the hybrid auxetic structure in the practical applications.

Keywords: auxetic structure; negative Poisson's ratio; mechanical property; re-entrant structure; parametric analysis

1 Introduction

As a class of mechanical meta-materials, auxetic structures have attracted an increasing attention during the past few decades due to their excellent mechanical properties such as enhanced shear modulus [1], better indentation resistance [2], improved fracture resistance [3], superior energy absorption ability [4], variable permeability [5], and unique synclastic behavior [6]. Different from conventional honeycomb structures with positive Poisson's ratio, auxetic structures have a negative Poisson's ratio (NPR) which

leads to an unusual deformation mechanism, that is, they transversely expand or contract when stretched or compressed in longitudinal direction [7]. Auxetic structures have been widely used in the field of mechanical engineering, civil engineering, chemical engineering, biomedicine, aerospace, and transportation [7-9].

In 1987, Lakes [1] first designed and fabricated an isotropic man-made foam with a NPR. Later, Evans [6] introduced "auxetics" to describe the counterintuitive deformation mechanism for convenience. Since the NPR behavior of auxetic structures stems from the internal architecture of the constituent unit cells [10], different basic auxetic unit cell geometries have been developed, such as chiral [12], rigid rotation [13], star-shaped [14], origami [15], kirigami [16], re-entrant [17], and double arrowhead [18] structures. In recent years, three strategies including inspiration from nature, topology optimization, and modification or combination of existing auxetic structures have been adopted by various researchers for the development of new auxetic structures to enhance their mechanical properties.

It is well-known that the biological materials possess superior properties and unique structures during the long-term evolution. Various researchers have focused their investigations on the bio-inspired auxetic structures. For example, Liu et al. [19] designed the multi-cell carbon fiber reinforced plastic and aluminum square tube with high specific energy-absorption by the inspiration of bamboo and coconut palm. Zou et al. [20] introduced the structure of bamboo to develop the thin-walled tube with the enhanced energy absorption. Huang and Xu proposed a bionic multi-cell tube for the impact protection inspired from the dactyl clubs structure of a marine crustacean named odontodactylus scyllarus [21]. Jiang et al. developed a concentric auxetic reentrant honeycomb inspired from the coconut palm to effectively absorb the impact energy [22]. Zhang et al. designed a re-entrant arc-shaped honeycomb inspired from the turtle shell structure to enhance the in-plane impact resistance [23]. As mentioned above, topology optimization method is also used in the design of auxetic structures. Wang proposed a subsequent shape optimization method through parametrizing material configurations using a set of super-ellipsoids for designing auxetic structures [24]. Radman et al. optimized the base cell to enhance bulk modulus or shear modulus of isotropic auxetic structures through the bidirectional evolutionary structural optimization technique [25]. Zheng et al. presented two numerical strategies on the sensitivity calculation and variable updating to stabilize the bidirectional evolutionary structural optimization process of auxetic structures [26]. Kaminakis and Stavroulakis used the evolutionary-hybrid algorithm as topology optimization method to design auxetic materials [27]. Nguyen et al. investigated three-dimensional topology optimization of auxetic meta-material through isogeometric analysis and model order reduction [28]. Yang et al. proposed a novel class of mechanical meta-materials based on topology analysis with the existing auxetic cellular structures [29]. Zhang et al developed a bi-material microstructure design method for the chiral auxetic metamaterial using topology optimization [30].

Compared with the above two design method, developing the auxetic structures through modification or combination of existing auxetic structures has received special attention due to the chance of nature inspiration and the shape irregularity of the topology

optimization. Xu et al. [31] proposed a 2D hybrid AuxHex structure comprising of re-entrant auxetic and hexagonal honeycomb cells. Compared with re-entrant auxetic or hexagonal honeycomb structures, the hybrid 2D AuxHex structure exhibits better mechanical properties and energy absorption [32]. A 3D lattice AuxHex structure consisting of auxetic re-entrant and hexagonal components was designed by Guo et al. [33]. Zhang et al investigated the in-plane mechanical behavior of a novel auxetic hybrid meta-material combining a core unit cell of re-entrant and lateral missing ribs [34]. Gao et al. designed and fabricated a carbon fiber reinforced composite 3D auxetic lattice structure by embedding the longitudinal supporting ribs into the arrowhead cell [35]. Qi et al. proposed a novel re-entrant circular honeycomb configuration by replacing the sloped cell wall of the regular re-entrant honeycomb with double circular arc cell walls [36]. Lv et al. presented a hierarchical octet-truss lattice structure by replacing the solid strut of the octet-truss structure with a tubular re-entrant structure [37]. Logakannan et al. developed a re-entrant diamond structure comprising of re-entrant auxetic and diamond-shaped honeycomb cells [38]. Guo et al. designed a double-U auxetic honeycomb structure based on the double-arrowhead structure [39]. Zhang et al. developed a star-re-entrant hierarchical meta-material based on a re-entrant representative unit cell consisting of star-shaped subordinate cells [40].

In this paper, a novel type of hybrid auxetic structure by combining unit cells of two basic auxetic geometries is proposed. Since the re-entrant and double-arrowhead honeycomb structures show larger effective Young's modulus than other basic auxetic honeycombs of equal mass [11], the novel hybrid auxetic structure will be designed by combining the unit cells of these two structures, to achieve better mechanical properties and a wider range of Poisson's ratio from negative to the positive. The paper is organized as follows. In Section 2, the hybrid auxetic structure is designed and its theoretical analysis model is developed. The parametric study on the in-plane mechanical properties of the hybrid structure is described in Section 3. Comparison of the hybrid and re-entrant structures is conducted in Section 4. The experimental measurements are shown in Section 5. Conclusions are summarized in Section 6.

2 Structure design and theoretical analysis

2.1 Structure design

An auxetic lattice structure deforms by either bending or stretching of its cell walls. Compared with the bending-dominated structure, the stretching-dominated auxetic structure possesses the higher stiffness [41,42]. In order to judge the dominated deformation behavior, an auxetic structure can be assumed as a pin-jointed frame, i.e., it is comprised of an infinite number of unit cells and the internal struts and connected through frictionless pin joints. A pin-jointed frame is considered to be rigid if it is both statically and kinematically determinate. As suggested by Maxwell [43], the judging criteria are necessary conditions rather than general sufficient conditions, as the possibility of states of self-stress (a self-equilibrated state of strut tensions in the absence of external load) and one mechanism is not taken into consideration. When the equivalent pin-jointed frame of an auxetic structure is not rigid, it tends to have the

bending deformation under external forces. According to Maxwell's criteria, the necessary condition for rigidity is that an average connectivity (number of struts at a node) of the frame is not lower than 4 [43]. As shown Figure 1(a), the average connectivity of the re-entrant auxetic structure is 3, which does not satisfy Maxwell's criteria, and thus, it is not rigid. The average connectivity of the double-arrowhead auxetic structure (see Figure 1(b)) is 4 and it admits one mechanism and one state of self-stress. Thus, though Maxwell's criteria are satisfied, it is a movable mechanism and not rigid. As mentioned above, among the basic auxetic structures, the re-entrant and double-arrowhead structures possess higher elasticity modulus, but they still belong to the bending-dominated deformation structures.

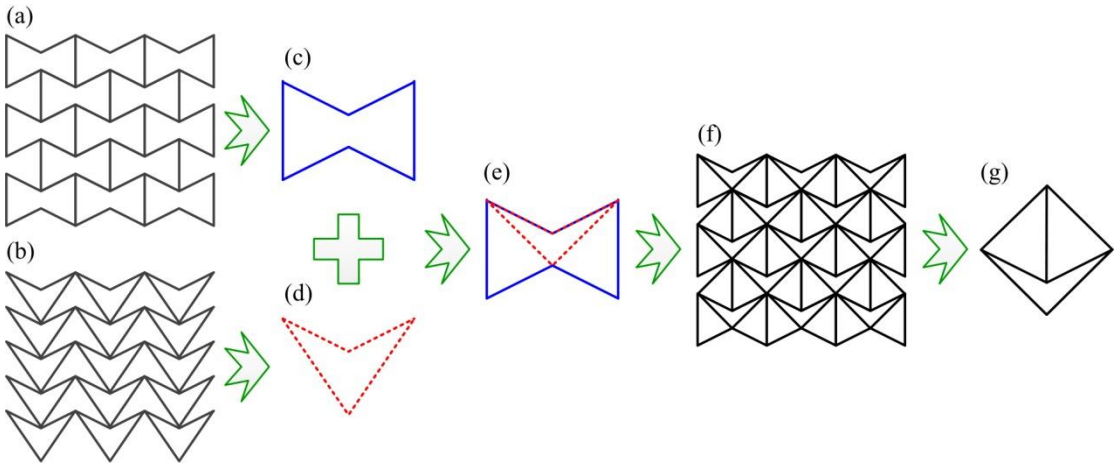

Figure 1. Design process of the hybrid auxetic structure.

Based on the stretching-dominated structure design concept, this work develops a hybrid auxetic structure by combining the re-entrant unit cell (Figure 1 (c)) and the double-arrowhead unit cell (Figure 1 (d)). As shown in Figure 1(e), the two unit-cells are fitted together and the arrowhead with the large angle in the double-arrowhead unit cell is coincident with the inclined walls in the re-entrant unit cell. The combined hybrid auxetic structure is shown in Figure 1 (f) and its unit cell is shown in Figure 1 (g). From Figure 1(g), it can be seen that the number of the average connectivity is 4 when the hybrid auxetic structure is regarded as a pin-jointed frame, which satisfies the Maxwell criteria. Besides, the hybrid structure is not one mechanism or at the state of self stress. Thus, the developed hybrid structure is stretching-dominated.

2.2 Theoretical analysis

As shown in Figure 2, the periodic auxetic structure is comprised of three types of walls. The active length and center line length of the vertical wall are l_0 and l_{s1}, respectively, and the corresponding thickness is t_0. The active length of the inclined wall in the external quadrilateral frame of the hybrid unit cell is l_1 and the corresponding inclined angle is θ_1. The active length of the inclined wall in the internal arrowhead part is l_2 and the corresponding inclined angle is θ_2. The thickness of two types of the inclined walls is t_1 and t_2, respectively. The length of the hybrid unit cell in the horizontal direction is l_{s2}. The thickness of the hybrid structure in the direction perpendicular to the x-y plane

is set as b.

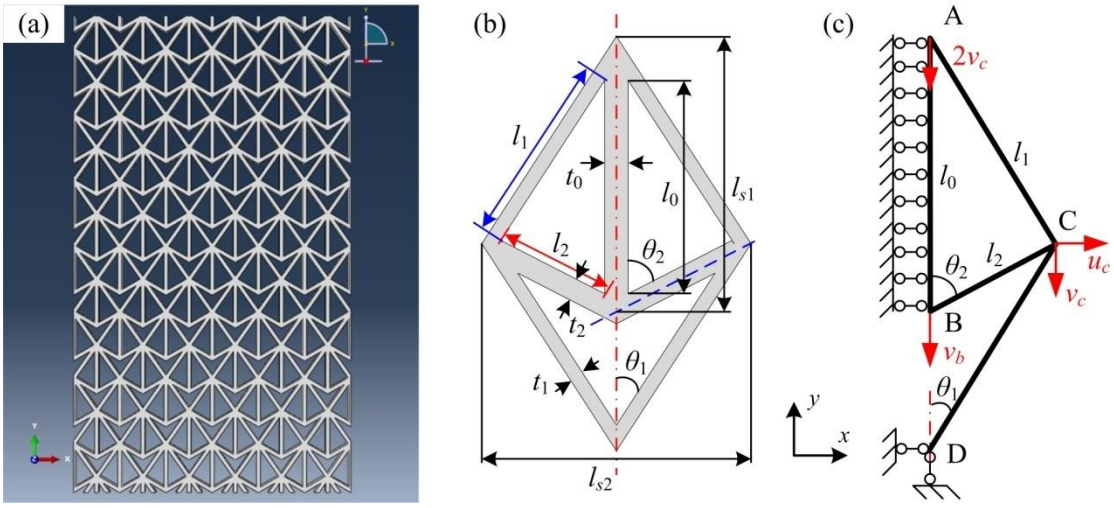

Figure 2. (a) The sketch of the hybrid auxetic structure, (b) The unit cell of the hybrid auxetic structure, and (c) the deformation behavior of the half unit cell under the static load.

Considering the overlapping area of the walls at each node (see Figure 3), the relative density of an infinite hybrid auxetic structure is found as follows.

$$rp = \frac{\left(\begin{array}{l} \dfrac{l_0 t_0}{2} + l_1 t_1 + l_2 t_2 + \dfrac{t_0^2}{8}\left(\dfrac{1}{\tan\alpha_0} + \dfrac{1}{\tan\alpha_6}\right) \\ + \dfrac{t_1^2}{8}\left(\dfrac{3}{\tan\alpha_5} + \dfrac{3}{\tan\alpha_7} - \dfrac{1}{\tan\alpha_2} - \dfrac{1}{\tan\theta_1}\right) \\ + \dfrac{t_2^2}{8}\left(\dfrac{3}{\tan\alpha_1} + \dfrac{3}{\tan\alpha_4} - \dfrac{1}{\tan\alpha_3} + \dfrac{1}{\tan\theta_2}\right) \end{array}\right)}{\left(l_1 + \dfrac{t_1}{2\tan\alpha_5} + \dfrac{t_1}{2\tan\alpha_7}\right)^2 \sin\theta_1 \cos\theta_1}, \tag{1}$$

where the angle α_i (i=1,2,…, 7) can be obtained by the geometrical relationship of the overlaps at the nodes. In order to ensure that the intersection angle at node A is θ_1 (the intersection of the vertical wall and the inclined wall in the external quadrilateral frame of the hybrid unit cell) rather than θ_2 (the intersection of the vertical wall and the inclined wall in the internal arrowhead part of the hybrid unit cell), the geometric constraint needs to be satisfied

$$\frac{1}{\tan\alpha_6} \geq \frac{1}{\tan\alpha_0}, \tag{2}$$

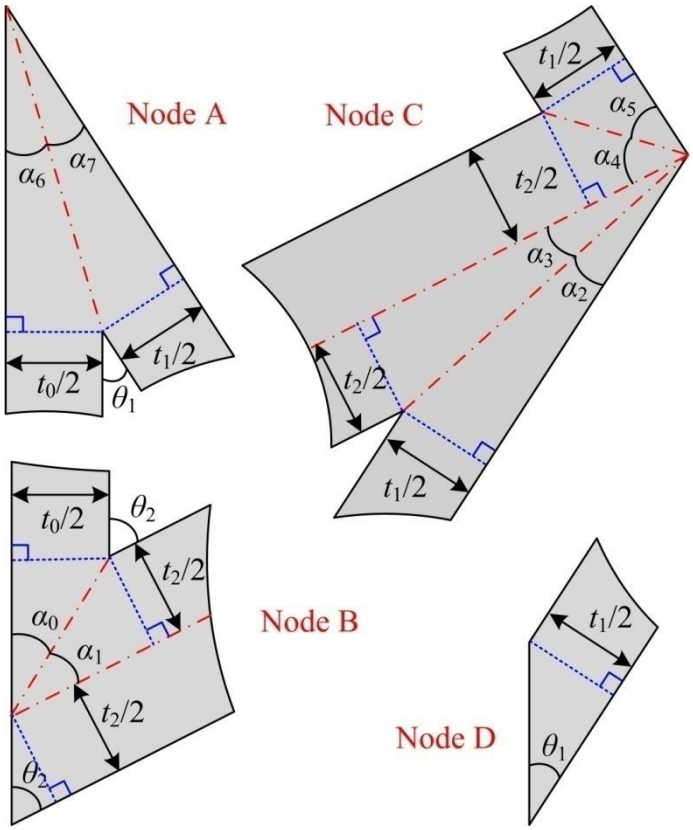

Figure 3. The geometrical relationship of the overlaps at the nodes.

The elastic properties of the hybrid auxetic structure are theoretically investigated based on the first-order shear deformation beam theory. According to the symmetric geometry, it can be concluded that mechanical properties of the developed hybrid structure along the vertical direction are completely identical, and thus, the theoretical analysis is performed on the half unit cell, as described as Figure 2 (c). The parent material properties of the three types of walls are, respectively, denoted as E_0, μ_0, G_0, E_1, μ_1, G_1 and E_2, μ_2, G_2. In this analysis, the force constant of the wall is defined for simplifying the theoretical expressions. The force constant of the vertical wall is

$$K_0 = \frac{1}{\frac{l_0}{E_0 b t_0}}, \tag{3}$$

and the force constants of two types of the inclined walls are expressed as

$$\begin{cases} K_i^a = \dfrac{\sin^2\theta_i}{\dfrac{l_i}{E_i bt_i}} + \dfrac{\cos^2\theta_i}{\dfrac{l_i}{kG_i bt_i} + \dfrac{l_i}{12E_i I_i}} \\ K_i^b = \dfrac{\sin\theta_i\cos\theta_i}{\dfrac{l_i}{kG_i bt_i} + \dfrac{l_i}{12E_i I_i}} - \dfrac{\sin\theta_i\cos\theta_i}{\dfrac{l_i}{E_i bt_i}} \\ K_i^c = \dfrac{\cos^2\theta_i}{\dfrac{l_i}{E_i bt_i}} + \dfrac{\sin^2\theta_i}{\dfrac{l_i}{kG_i bt_i} + \dfrac{l_i}{12E_i I_i}} \end{cases} \tag{4}$$

where l_i, t_i, and θ_i (i=1, 2) are geometric parameters of the hybrid unit cell, and $I_i = bt_i^3/12$ is inertia moment of the rectangular cross-section, and k=5/6 is the shear coefficient of the rectangular cross-section.

Figure 2(c) demonstrates the deformation behavior of the half hybrid auxetic unit cell under a uniform tensile (compressive) load along a principal direction. In order to simplify the analysis, the node D is assumed to be fixed. Due to the symmetric geometry, the displacement of nodes A and B along the horizontal direction is also fixed. The deformation behavior in Figure 2 is described through three nodal displacement parameters. The displacement of the node C in the horizontal and vertical direction is u_c and v_c, respectively. The displacement of the nodes A and B in the vertical direction is $2v_c$ and v_b.

It is assumed that only the axial force is in the vertical wall and its deformation is uniformly distributed. The vertical nodal force of the wall AB at the node B can be expressed as

$$F_{AB}^y = \frac{1}{2}K_0\left(2v_c - v_b\right), \tag{5}$$

The deformation of the inclined wall is comprised of the axial, bending, and shear deformation. Based on the first-order shear deformation beam theory, the horizontal and vertical nodal forces of the wall DC at the node D are expressed as

$$\begin{cases} F_{DC}^x = \dfrac{1}{2}\left(K_1^a u_c + K_1^b v_c\right) \\ F_{DC}^y = \dfrac{1}{2}\left(K_1^b u_c + K_1^c v_c\right) \end{cases}, \tag{6}$$

Similarly, the horizontal and vertical nodal forces of the wall BC at the node B are given as

$$\begin{cases} F_{BC}^x = K_2^a u_c + K_2^b\left(v_c - v_b\right) \\ F_{BC}^y = K_2^b u_c + K_2^c\left(v_c - v_b\right) \end{cases}, \tag{7}$$

Since the angle of the wall AC is π-θ_1， the nodal forces of the wall AC at the node A along the horizontal and vertical directions are given as

$$\begin{cases} F_{AC}^{x} = \dfrac{1}{2}\left(K_1^a u_c + \left(-K_1^b\right)\left(v_c - 2v_c\right)\right) \\ F_{AC}^{y} = \dfrac{1}{2}\left(-K_1^b u_c + K_1^c\left(v_c - 2v_c\right)\right) \end{cases}, \tag{8}$$

Three loading cases are considered in this analysis. The first case is that only the uniform stress σ_y in the vertical direction is applied to the hybrid auxetic structure. When the hybrid structure is in an equilibrium state, the force equilibrium condition on the boundary of the half unit cell as well as at each node should be met. In this case, according to the force balance at the node B in the vertical direction, it can be obtained as

$$2\left(F_{AB}^{y} + F_{BC}^{y}\right) = 0, \tag{9}$$

Since the hybrid structure is free in the horizontal direction, the resultant force of the half unit cell is equal to zero, namely,

$$F_{DC}^{x} + F_{BC}^{x} + F_{AC}^{x} = 0, \tag{10}$$

According to equations (3)-(6), all the nodal forces in equations (9) and (10) can be expressed as functions of the nodal displacements. After substituting equations (5)-(8) into equations (9) and (10), u_c and v_b can be expressed as a function of v_c, which can be written as

$$\begin{cases} u_c = \dfrac{2\left(K_0 + K_2^c\right)K_2^b - \left(K_1^b + K_2^b\right)\left(K_0 + 2K_2^c\right)}{\left(K_0 + 2K_2^c\right)\left(K_1^a + K_2^a\right) - 2\left(K_2^b\right)^2} v_c \\ v_b = \dfrac{2\left(K_1^a + K_2^a\right)\left(K_0 + K_2^c\right) - 2\left(K_1^b + K_2^b\right)K_2^b}{\left(K_0 + 2K_2^c\right)\left(K_1^a + K_2^a\right) - 2\left(K_2^b\right)^2} v_c \end{cases}, \tag{11}$$

Similarly, the resultant force of the half unit cell in the horizontal direction should be equal to the applied external force, namely,

$$F_{AB}^{y} - 2F_{AC}^{y} = \frac{1}{2}\sigma_y b l_{s2}, \tag{12}$$

Substituting equations (5) and (8) into equation (12), the stress σ_y can be expressed as

$$\sigma_y = \frac{1}{b l_{s2}}\left(2K_1^b \frac{u_c}{v_c} - K_0 \frac{v_b}{v_c} + 2K_1^c + 2K_0\right) v_c, \tag{13}$$

The Young's modulus of the hybrid auxetic structure in the vertical direction can be written as

$$E_y = \frac{\sigma_y}{\varepsilon_y} = \frac{\sigma_y}{2v_c/2l_1\cos\theta_1}$$
$$= \frac{l_1\cos\theta_1}{bl_{s2}}\left(\begin{array}{l} 2K_1^b\dfrac{2\left(K_0+K_2^c\right)K_2^b-\left(K_1^b+K_2^b\right)\left(K_0+2K_2^c\right)}{\left(K_0+2K_2^c\right)\left(K_1^a+K_2^a\right)-2\left(K_2^b\right)^2}+2K_0 \\ -K_0\dfrac{2\left(K_1^a+K_2^a\right)\left(K_0+K_2^c\right)-2\left(K_1^b+K_2^b\right)K_2^b}{\left(K_0+2K_2^c\right)\left(K_1^a+K_2^a\right)-2\left(K_2^b\right)^2}+2K_1^c \end{array}\right), \tag{14}$$

where ε_y is the strain in the vertical direction. Poisson's ratio of the hybrid auxetic structure in the vertical direction is expressed as follows

$$v_{yx} = -\frac{\varepsilon_x}{\varepsilon_y} = \frac{2u_c/l_{s2}}{2v_c/\left(2l_1\cos\theta_1\right)} = \frac{2l_1\cos\theta_1}{l_{s2}}\frac{2\left(K_0+K_2^c\right)K_2^b-\left(K_1^b+K_2^b\right)\left(K_0+2K_2^c\right)}{\left(K_0+2K_2^c\right)\left(K_1^a+K_2^a\right)-2\left(K_2^b\right)^2}, \tag{15}$$

The second loading case is that only the uniform stress σ_x in the horizontal direction is applied to the hybrid auxetic structure. Similar to the loading along the vertical direction, when the uniform stress σ_x in the horizontal direction is applied, the corresponding mechanical properties are also obtained by the force equilibrium condition. In this case, the force balance at the node B in the vertical direction still meets equation (9), and the resultant force of the half unit cell in the vertical direction is equal to zero, that is,

$$F_{AB}^y - 2F_{AC}^y = 0, \tag{16}$$

By solving the equilibrium equations (9) and (16), v_c and v_b can be derived as functions of u_c, namely,

$$\begin{cases} v_c = \dfrac{2\left(K_0+2K_2^c\right)K_1^b-2K_0K_2^b}{2\left(K_0+K_2^c\right)K_0-\left(2K_0+2K_1^c\right)\left(K_0+2K_2^c\right)}u_c \\ v_b = \dfrac{4K_1^b\left(K_0+K_2^c\right)-2\left(2K_0+2K_1^c\right)K_2^b}{2\left(K_0+K_2^c\right)K_0-\left(2K_0+2K_1^c\right)\left(K_0+2K_2^c\right)}u_c \end{cases}, \tag{17}$$

In addition, the resultant force of the half unit cell in the horizontal direction should be equal to the applied external force, which can be expressed as

$$2\left(F_{DC}^x + F_{BC}^x + F_{AC}^x\right) = \sigma_x bl_{s2}/\tan\theta_1, \tag{18}$$

Thus, the stress σ_x can be expressed as

$$\sigma_x = \frac{2\tan\theta_1}{bl_{s2}}\left(K_1^a+K_2^a+\left(K_1^b+K_2^b\right)\frac{v_c}{u_c}-K_2^b\frac{v_b}{u_c}\right)u_c, \tag{19}$$

In this case, the Young's modulus of the hybrid auxetic structure in the horizontal direction is found as

$$E_x = \frac{\sigma_x}{\varepsilon_x} = \frac{\sigma_x}{u_c / l_1 \sin\theta_1}$$
$$= \frac{2l_1 \tan\theta_1 \sin\theta_1}{b l_{s2}} \left(\begin{array}{l} K_1^a + K_2^a - K_2^b \dfrac{4K_1^b \left(K_0 + K_2^c\right) - 2\left(2K_0 + 2K_1^c\right) K_2^b}{2\left(K_0 + K_2^c\right) K_0 - \left(2K_0 + 2K_1^c\right)\left(K_0 + 2K_2^c\right)} \\ + \left(K_1^b + K_2^b\right) \dfrac{2\left(K_0 + 2K_2^c\right) K_1^b - 2K_0 K_2^b}{2\left(K_0 + K_2^c\right) K_0 - \left(2K_0 + 2K_1^c\right)\left(K_0 + 2K_2^c\right)} \end{array} \right), \quad (20)$$

where ε_x is the strain in the horizontal direction. Poisson's ratio in the horizontal direction is given as follows

$$\nu_{xy} = -\frac{\varepsilon_y}{\varepsilon_x} = \frac{2v_c / \left(l_{s2} / \tan\theta_1\right)}{u_c / \left(l_1 \sin\theta_1\right)}$$
$$= \frac{2l_1 \tan\theta_1 \sin\theta_1}{l_{s2}} \frac{2\left(K_0 + 2K_2^c\right) K_1^b - 2K_0 K_2^b}{2\left(K_0 + K_2^c\right) K_0 - \left(2K_0 + 2K_1^c\right)\left(K_0 + 2K_2^c\right)}, \quad (21)$$

The third loading case is that the hybrid auxetic structure is subjected to a uniform shear stress τ_{yx} in the vertical direction. For simplifying the analysis, it is assumed that the main deformation is from the inclined walls and there exists no deformation for the vertical walls. In addition, similar to the literature [35], the rotational displacement of all nodes is also ignored. Thus, the deformation of the half unit cell is determined by the displacement of the node C in the vertical direction, while the other nodes are fixed. Similarly, combining with the force equilibrium condition, the shear modulus of the hybrid auxrtic structure is obtained as follows

$$G_{xy} = \frac{2l_1 \tan\theta_1 \sin\theta_1}{b l_{s2}} \left(K_1^c + K_2^c - \frac{\left(K_2^b\right)^2}{K_1^a + K_2^a} \right), \quad (22)$$

3. Parametric analysis

In this section, the mechanical properties of the hybrid auxetic structure under diverse geometric parameters will be analyzed, aiming at exploring the effective method for the property improvement. Firstly, a finite element method (FEM) is used to develop a numerical simulation model of the hybrid auxetic structure for the verification of the developed theoretical analysis model. The finite element model is developed by using the commercial finite element modeling software ABAQUS and shown in Figure 4. As mentioned above, the first-order shear deformation beam theory is adopted in theoretical analysis, while the hexahedral solid element is selected for the finite element model. The mesh convergence test of the finite element model is performed before the formal numerical analysis. A comparison between the theoretical and numerical results of the normalized effective Young's modulus, shear modulus, and Poisson's ratio along the principal directions, when θ_2=60°, E_0=E_1=E_2=E, t_0=t_1=t_2=t, and l_{s1}=l_{s2}=l_s, is shown in Figure 5. It can be seen that the theoretical results agree well with the numerical results, which verify the viability of the developed theoretical model. In addition, it is also noticed that the errors between the theoretical and numerical results increase as the

value of l_s/t increases. The reason can be explained by the fact that with the decrease in the value of l_s/t, the overlapping effect at the nodes on the length of the wall is enhanced, and thus, leading to an increase of the errors between the theoretical prediction and numerical simulation.

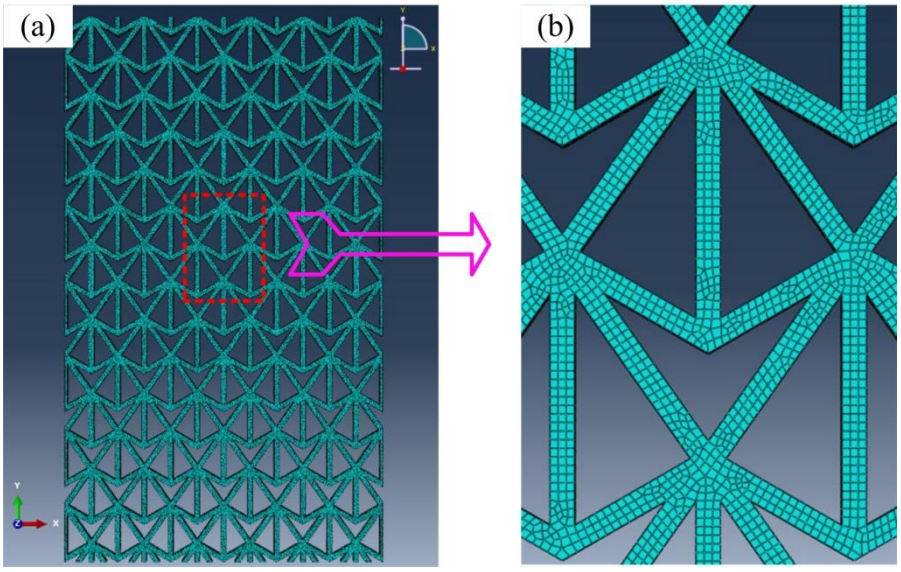

Figure 4. The sketch of the developed finite element model.

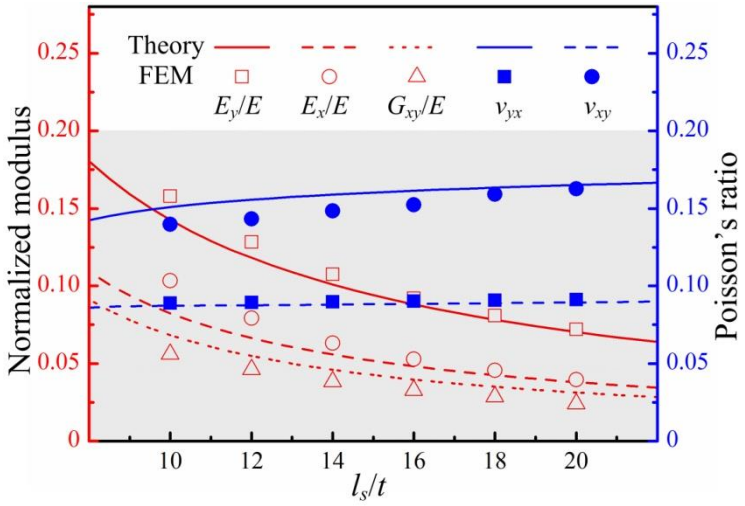

Figure 5. Comparison between theoretical and numerical results.

Using the verified theoretical model, the mechanical properties of the hybrid auxetic structure including effective moduli, Poisson's ratio, and relative density are calculated from different values of geometric parameters for parametric analysis. Figure 6 shows the effects of the parameters l_s/t and θ_2 on the mechanical properties of the hybrid auxetic structure when $E_0=E_1=E_2=E$, $t_0=2t_1=t_2=t$, and $l_{s1}=l_{s2}=l_s$. In this case, l_{s1} and l_{s2} are kept equal. The variation of the Young's modulus E_x in the horizontal direction is described in Figure 6 (a). It can be seen that as l_s/t decreases or θ_2 increases, E_x can be increased, indicating that the Young's modulus in the horizontal direction can be improved by reducing l_s/t and increasing θ_2. However, decreasing l_s/t can increase the relative density r_p (see Figure 6(f)), which leads to the weight increase of the hybrid

structure, while increasing θ_2 can decrease r_p, which contributes to reducing the weight of the hybrid structure. Figure 6 (b) displays the variation of the Young's modulus E_y in the vertical direction. Similarly, reducing l_s/t can also enhance the Young's modulus in the vertical direction. The main reason for this is that with the decrease in the length of the inclined wall, the rotational angle of its cross-section decreases under the same given force, resulting in less bending deformation. As a result, the modulus of the hybrid structure increases. Different from the variation of E_x, E_y can first increase and then decrease with the increase in the angle θ_2, exhibiting the non-monotonic behavior. It can be also noticed that at small l_s/t, after the peak is reached, E_y can slowly decline with the increase of θ_2, inferring that the high elasticity modulus can only be obtained at large θ_2. As shown in Figure 6 (c), the high shear modulus can be obtained at small l_s/t and θ_2. From the above analysis, it can be inferred that decreasing l_s/t can enhance the mechanical properties of the hybrid structure, including the elasticity moduli in the two principle directions and the shear modulus. The variations of Poisson's ratio in the horizontal and vertical directions are shown in Figure 6 (d) and 6(e), respectively. It can be also seen that Poisson's ratios in two directions can decrease with the increase of l_s/t, but their variations with θ_2 is in a non-monotonic way. When θ_2 is close 85°, the value of Poisson's ratio can transform from negative to positive, indicating that the hybrid structure can have three different deformation behaviors, i.e., negative, zero, and positive Poisson's ratio. Compared with the re-entrant and double-arrowhead structures, Poisson's ratio of the developed hybrid structure can be tunable in a wide range.

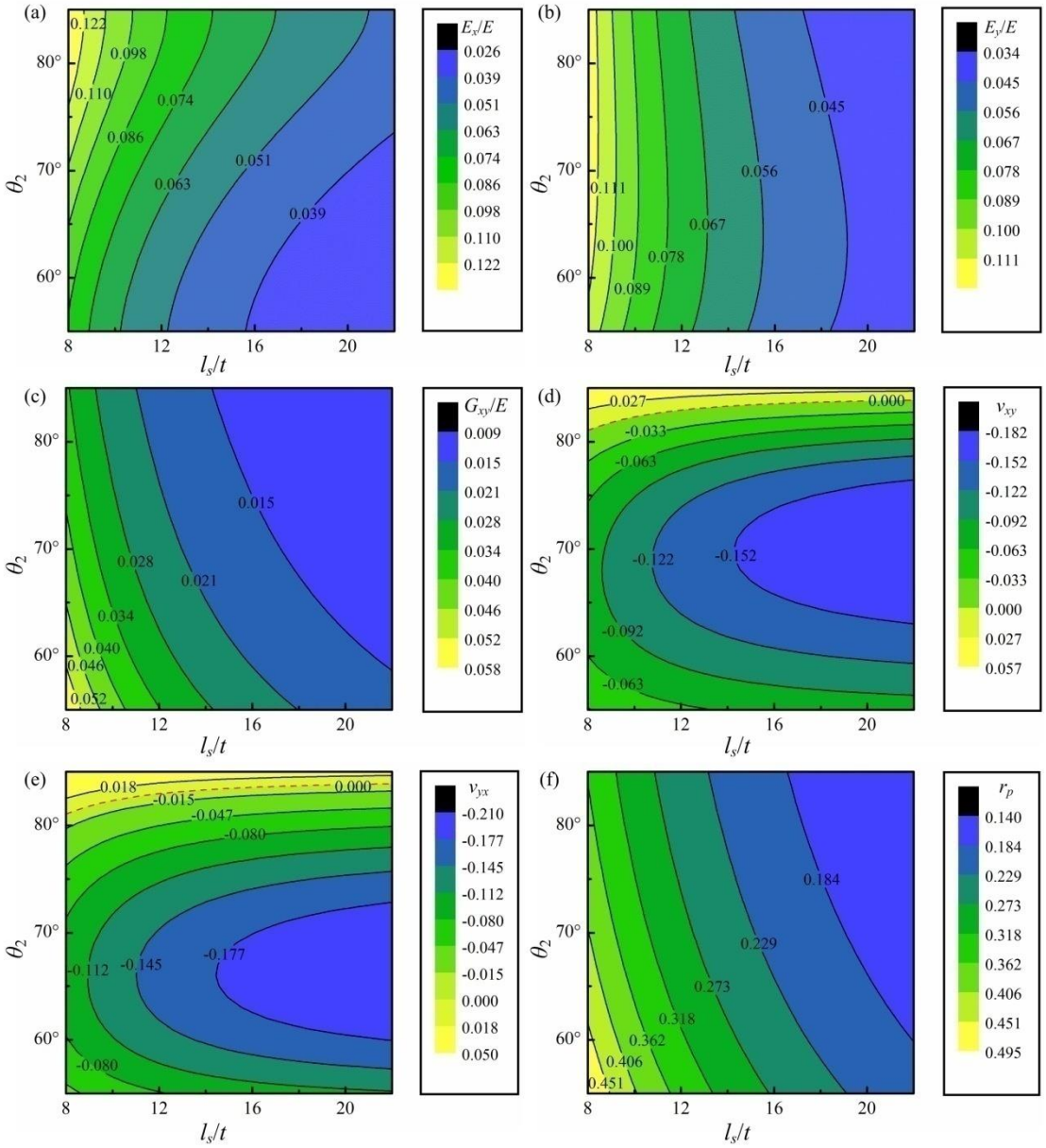

Figure 6. Effects of the parameters l_s/t and θ_2 on the mechanical properties of the hybrid auxetic structure.

Figure 7 shows the effects of the parameters l_{s1}/t and θ_2 on the mechanical properties of the hybrid auxetic structure when $E_0=E_1=E_2=E$, $t_0=2t_1=t_2=t$, and $l_{s2}/t=10$. In this case, l_{s1} and l_{s2} are no longer kept equal. In the figure, the gray area indicates the geometric incompatibility which does not satisfy the formula (2). It can be seen from Figure 7 (a) that E_x can be enhanced by increasing θ_2 or decreasing l_{s1}/t. The main reason is that as θ_2 increases, the inclined wall of the internal arrowhead part is gradually close to the horizontal direction, leading to the increase of E_x. On the other hand, with the decrease of l_{s1}, the inclined angle θ_1 can increase and the inclined wall in the external quadrilateral frame gradually trends to the horizontal direction, and thus, the modulus E_x can also increase. Different from the monotonic behavior of E_x, the variation of E_y with θ_2 is complicated, depending on l_{s1}/t (see Figure 7 (b)). At large l_{s1}/t, E_y can

decrease with the increase of θ_2, revealing that reducing θ_2 can improve the Young's modulus in the vertical direction. However, at small l_{s1}/t, the variation of E_y exhibits the non-monotonic behavior. From Figure 7 (b), it can be also seen that increasing l_{s1}/t can improve the Young's modulus in the vertical direction. Based on the above analysis, it can be found that the high modulus E_x can be achieved at small l_{s1}/t and large θ_2, while the high modulus E_y can be obtained at large l_{s1}/t and small θ_2. Thus, the difference of the elasticity moduli between the two principal directions can be obtained by adjusting l_{s1}/t and θ_2. As shown in Figure 7(d), the variation of Poisson's ratio v_{xy} with l_{s1}/t can be affected by θ_2. At small θ_2, v_{xy} can first decrease and then increase with the increase of l_{s1}/t, and thus, there is an optimal l_{s1}/t to minimize v_{xy}. At large θ_2, as l_{s1}/t increases, v_{xy} can decrease from positive to negative, indicating that increasing l_{s1}/t contributes to enhancing the NPR effect of the hybrid structure. It can be also noticed from Figure 7 (d) that the variation of v_{xy} with θ_2 exhibits the non-monotonic behavior. As shown in Figure 7 (e), at small l_{s1}/t, Poisson's ratio v_{yx} can first decrease and then increase with the increase of θ_2. However, at large l_{s1}/t, the variation of v_{yx} with θ_2 becomes monotonic. It can be also seen that increasing l_{s1}/t can reduce v_{yx}. Through the above analysis, it can be found that both the high elastic modulus and the NPR effect in the vertical direction can be achieved by increasing l_{s1}/t and decreasing θ_2. At the same time, the hybrid structure can still keep a low relative density (see Figure 7(f)).

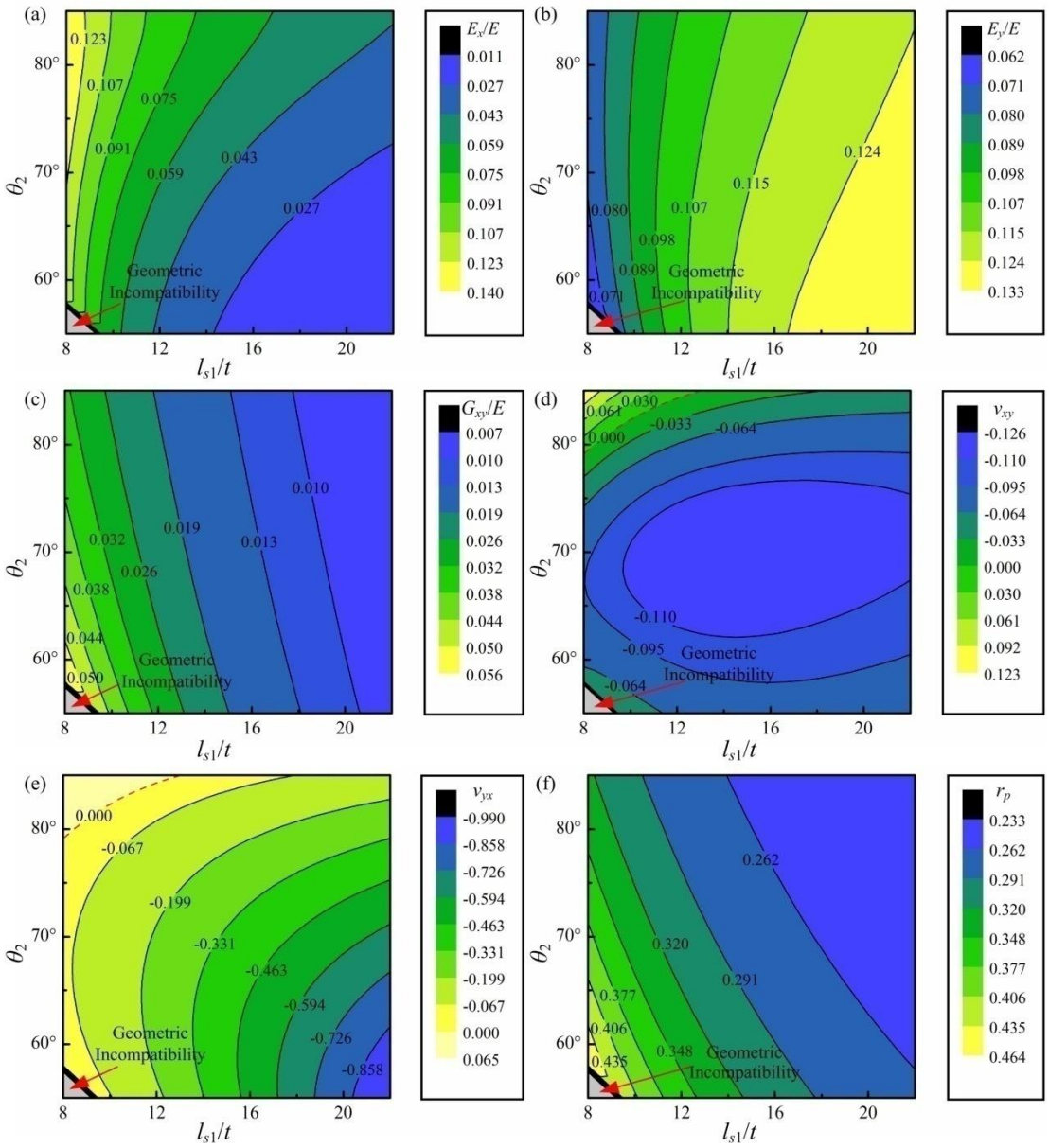

Figure 7. Effects of the parameters l_{s1}/t and θ_2 on the mechanical properties of the hybrid auxetic structure.

Figure 8 shows the effects of the parameters l_{s2}/t and θ_2 on the mechanical properties of the hybrid auxetic structure when $E_0=E_1=E_2=E$, $t_0=2t_1=t_2=t$, and $l_{s1}/t=10$. The gray area of Figure 8 represents the area of the geometric incompatibility, in which the formula (2) is not satisfied. From Figure 8 (a) and (b), it can be seen that with the increase of l_{s2}/t, E_x can increase, while E_y can decrease. Thus, adjusting l_{s2}/t is also a feasible way to differentiate the elastic moduli between the two principal directions. The main reason can be explained as follows. As l_{s2} increases, θ_1 can also increase and the inclined wall in the external quadrilateral frame gradually trends to the horizontal direction. As a result, E_x tends to increase while E_y tends to decrease. From Figure 8 (a), it can be also noticed that increasing θ_2 can enhance the modulus in the horizontal direction at small l_{s2}/t, but reduce the modulus in the horizontal direction at large l_{s2}/t. When l_{s2}/t is at

intermediate value, the variation of E_x with θ_2 is found to be non-monotonic. Different from the obvious influence of θ_2 on E_x, θ_2 is not sensitive to E_y, as shown in Figure 8 (b). For the Poisson's ratios in the two principal directions, it can be seen from Figure 8 (d) and (e) that they can first decrease and then increase with the increase of θ_2 at the small l_{s2}/t, but have the monotonic behavior at large l_{s2}/t. Figure 8 (e) also displays that at small angle θ_2, v_{yx} can increase with the increase of l_{s2}/t, while at the large angle θ_2, the variation of v_{yx} with l_{s2}/t becomes non-monotonic. The variation of v_{xy} with l_{s2}/t is complex, and can be significantly affected by θ_2. The variation of v_{xy} with l_{s2}/t is monotonic at small or large θ_2, but shows the non-monotonic behavior at intermediate l_{s2}/t. From the above analysis, it can be found that the hybrid structure with both high elasticity modulus and NPR effect in the vertical direction can be obtained at small l_{s2}/t and θ_2, but this can cause high relative density (see Figure 8 (f)).

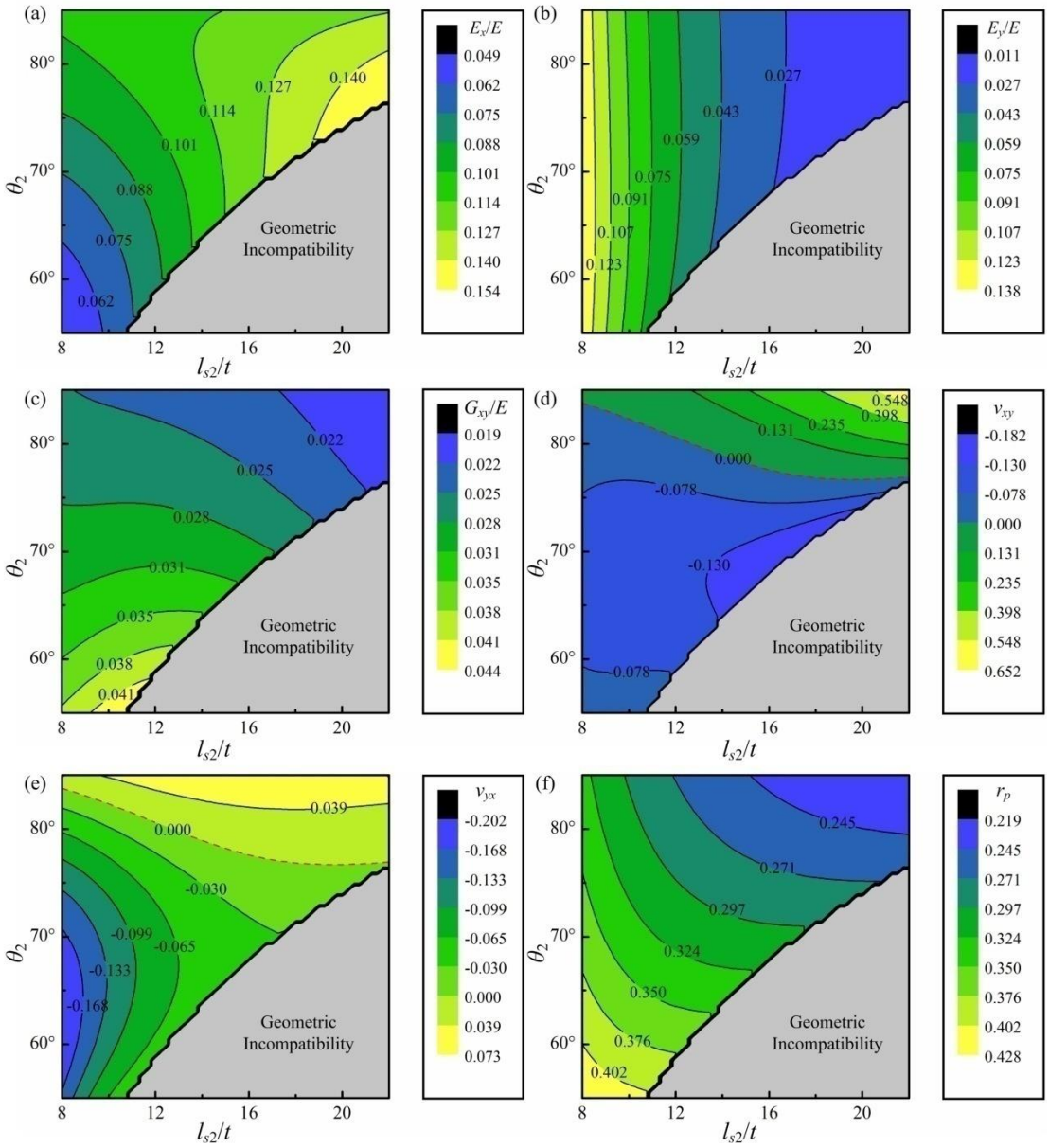

Figure 8. Effects of the parameters l_{s2}/t and θ_2 on the mechanical properties of the hybrid auxetic structure.

Figure 9 shows the effects of the parameters l_{s1}/t and t_1/t on the mechanical properties of the hybrid auxetic structure when $\theta_2=60^{\circ}$, $E_0=E_1=E_2=E$, $t_0=t_2=t$, and $l_{s2}/t=10$. Similarly, the gray area in Figure 9 belongs to the area of the geometric incompatibility. As shown in Figure 9 (a) and (b), as l_{s1}/t increases, E_x can decrease, but E_y can increase. Their variations are not affected by t_1/t. It can be also seen that increasing t_1/t can improve the elasticity moduli in the two principal directions. From Figure 9 (d), it can be seen that as l_{s1}/t increases, v_{xy} can increase at small t_1/t, but v_{xy} can decrease at large t_1/t. At intermediate t_1/t, the variation of v_{xy} with l_{s1}/t becomes non-monotonic. However, the variation of v_{yx} with l_{s1}/t exhibits the monotonic behavior, and is not affected by t_1/t (see Figure 9 (e)). In addition, increasing the t_1/t can increase values of v_{xy} and v_{yx}, causing a decrease of NPR effect. The main reason for this can be explained as follows. The NPR effect of the hybrid structure is mainly determined by the internal arrowhead part in the unit cell. When the thickness of the external quadrilateral frame increases, the influence of the internal arrowhead part can be weakened, and thus, Poisson's ratio value of the hybrid structure can increase. As shown in Figure 9 (f), increasing l_{s1}/t and decreasing t_1/t can reduce the relative density.

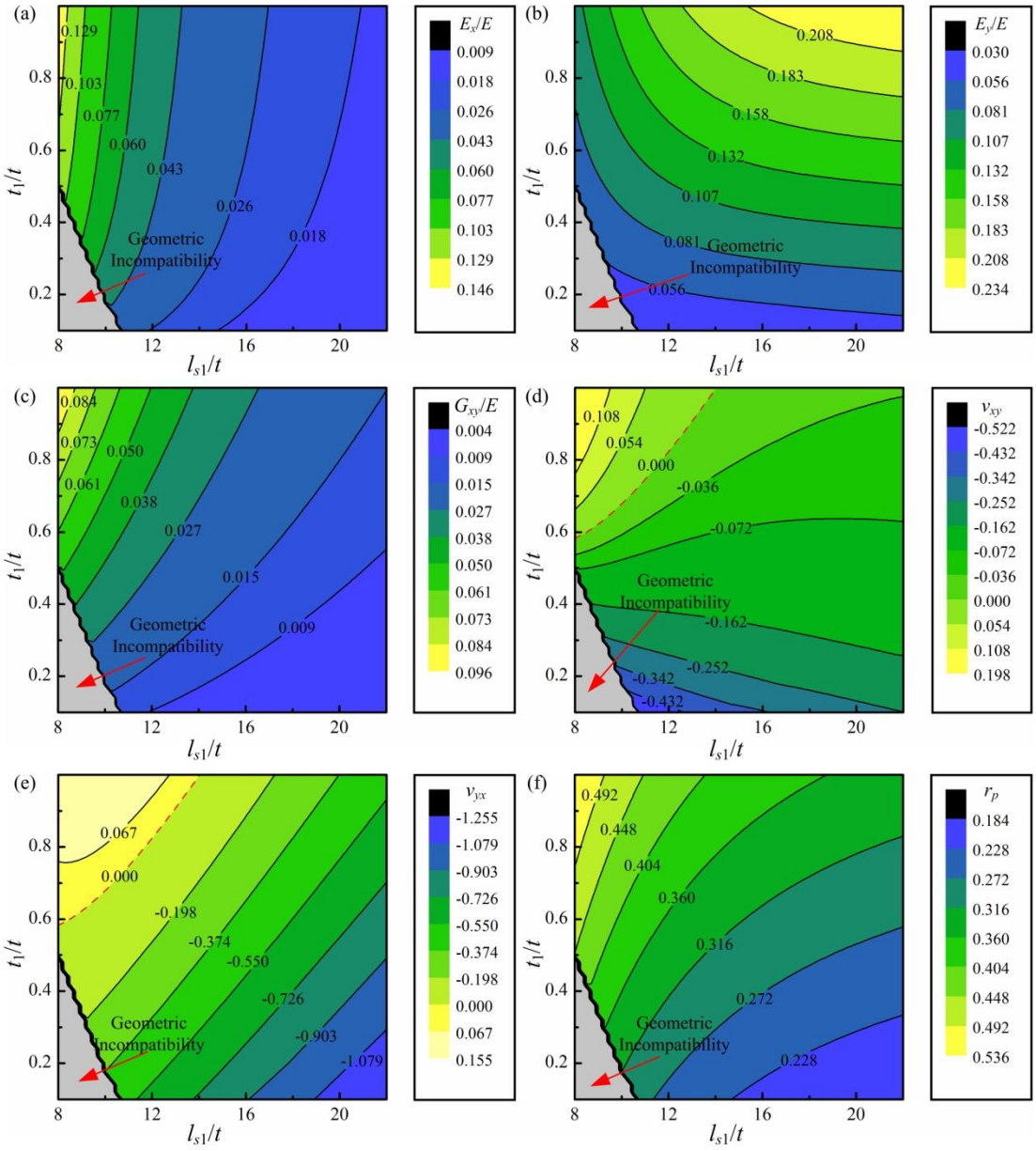

Figure 9. Effects of the parameters l_{s1}/t and t_1/t on the mechanical properties of the hybrid auxetic structure.

4 Comparison with re-entrant structures

In this section, the mechanical properties of the hybrid auxetic structure in the principal directions are compared with the re-entrant structure. First, the mechanical properties of the hybrid auxetic structure and the re-entrant structure with the same arrowhead geometric dimensions (the geometric dimensions of the internal arrowhead part in the unit cell of the hybrid auxetic structure are kept the same as those of the arrowhead unit cell of re-entrant structure.) are analyzed under different parameters l_{s1}/t and t_1/t, when θ_2=60°, E_0=E_1=E_2=E, t_0=t_2=t, and l_{s2}/t=10, as shown in Figure 10. As mentioned above, though increasing l_{s1}/t can enhance the modulus E_x of the hybrid structure, the relative density can also increase, indicating that this method for enhancing E_x is at the cost of increasing the relative density. In view of this, the specific modulus, the ratio of the

modulus and the mass density, is utilized for the evaluation of the mechanical properties. Figure 10 (a) displays the dimensionless specific elasticity moduli of the hybrid auxetic structure and the re-entrant structure in the horizontal direction. It can be seen that both the specific moduli of the hybrid structure and the re-entrant structure in the horizontal direction can increase with the decrease of l_{s1}/t. It can be also seen that as the thickness t_1 increases, the specific modulus of the hybrid structure in the horizontal direction can first increase and then decrease, revealing that there is an optimal thickness t_1 to maximize the specific modulus. Since the inclined wall in the external quadrilateral frame of the hybrid unit cell is not included in the re-entrant structure, the specific modulus remains constant at different t_1 (see Figure 10 (a), (b), and (c)). From Figure 10 (b), we can that increasing l_{s1}/t can enhance both the specific moduli of the hybrid structure and the re-entrant structure in the vertical direction. It can be also noticed that the specific modulus of the hybrid structure in the vertical direction can be also improved by increasing t_1/t. Figure 10 (c) describes the dimensionless specific shear modulus of the hybrid auxetic structure and the re-entrant structure. It can be observed that reducing l_{s1}/t or increasing t_1/t can improve the specific shear modulus of the hybrid structure. In addition, from Figure 10, we can see that the specific modulus of the hybrid structure is obviously higher than that of the re-entrant structure, indicating that the developed hybrid structure possesses the better mechanical property. Figure 11 shows Poisson's ratios of the hybrid auxetic structure and the re-entrant structure with the same arrowhead geometric dimensions under different l_{s1}/t and t_1/t. As shown in Figure 11 (a), at small t_1/t, the NPR effect of the hybrid structure in the horizontal direction is more obvious than that of the re-entrant structure, implying that the developed hybrid structure can obtain both high mechanical property and NPR effect in the horizontal direction. In addition, compared with the re-entrant structure, the hybrid structure has a wider range of Poisson's ratio from negative to positive.

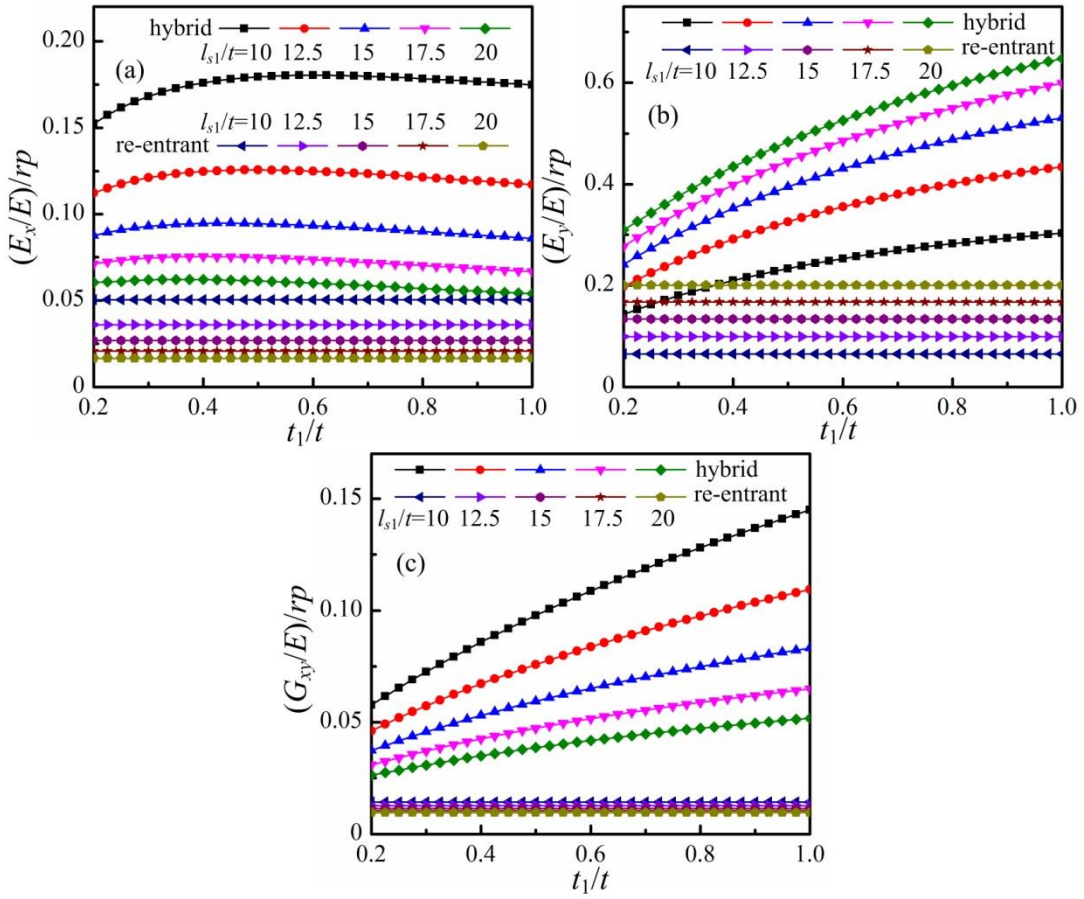

Figure 10. Comparison of mechanical properties of the hybrid auxetic structure and the re-entrant structure with the same arrowhead geometric dimensions under different parameters l_{s1}/t and t_1/t.

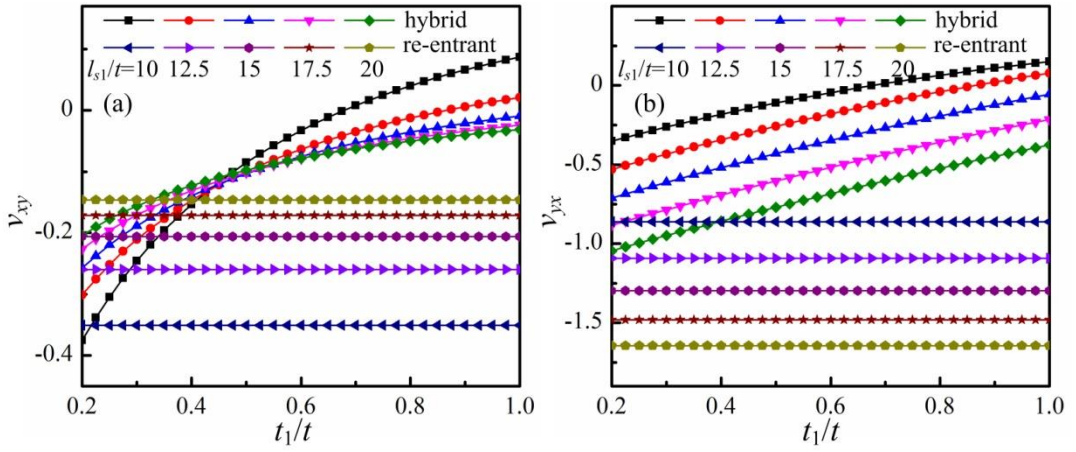

Figure 11. Comparison of Poisson's ratios of the hybrid auxetic structure and the re-entrant structure with the same arrowhead geometric dimensions under different parameters l_{s1}/t and t_1/t.

Then, the mechanical properties of the hybrid auxetic structure and the re-entrant structure with the same relative density are also analyzed under different l_{s1}/t and t_1/t, when θ_2=60°, E_0=E_1=E_2=E, t_0=t_2=t, and l_{s2}/t=10, for the hybrid structure, and θ_2=60°, E_0=E_1=E_2=E, t_0=t_2, and l_{s2}/t=10 for the re-entrant structure. The results are shown in

Figure 12. It should be noted that for the same relative density, t_0 and t_2 in the re-entrant structure can be changed, but for the hybrid structure, different l_{s1}/t and t_1/t can be given. As demonstrated in Figure 12, the moduli of the hybrid structure and the re-entrant structure can increase with the increase of t_1/t. It can be also seen that as l_{s1}/t increases, both E_x and G_{xy} can decrease, while E_y can increase. Figure 13 shows Poisson's ratios of the hybrid auxetic structure and the re-entrant structure with the same relative density under different l_{s1}/t and t_1/t. Similar with the case with the same arrowhead geometric dimensions, at small t_1/t, the hybrid structure has the higher NPR effect in the horizontal direction for this case. In addition, from Figure 12 and 13, we can notice that compared with the re-entrant structure, the hybrid structure possesses the better mechanical property and the wider and tunable range of Poisson ratios.

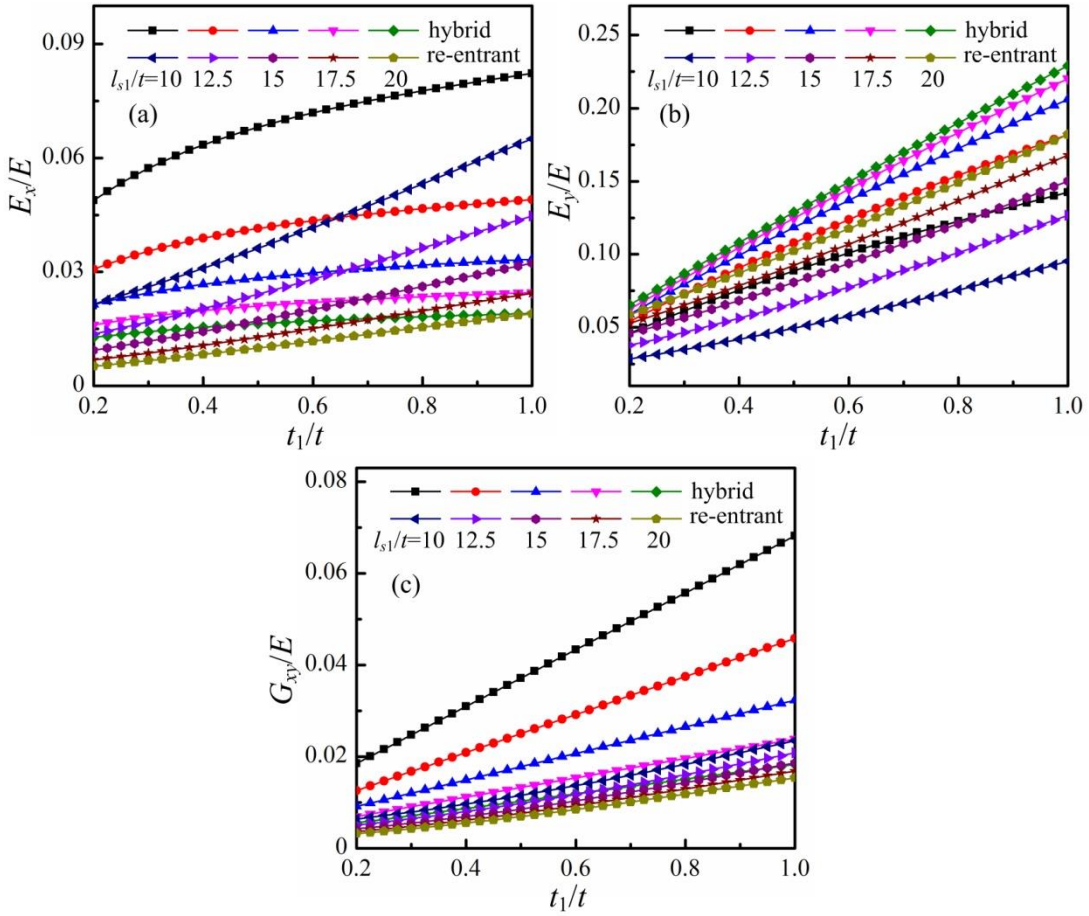

Figure. 12 Comparison of mechanical properties of the hybrid auxetic structure and the re-entrant structure with the same relative density under different parameters l_{s1}/t and t_1/t.

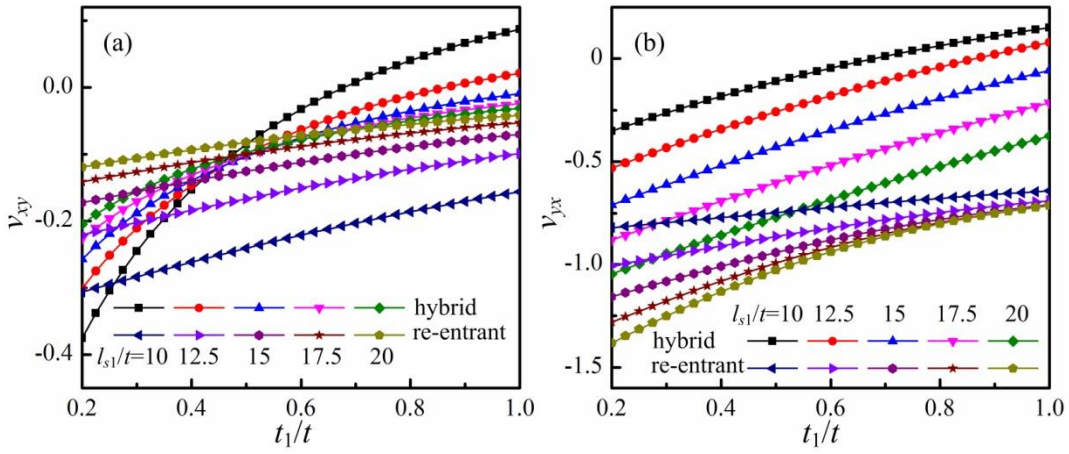

Figure 13. Comparison of Poisson's ratios of the hybrid auxetic structure and the re-entrant structure with the same relative density under different parameters l_{s1}/t and t_1/t.

5 Experimental Verification

Polylactic acid (PLA) was used as the parent material to fabricate the experimental samples through the 3D printing technology. The mechanical properties of the PLA material were measured by the uniaxial tensile test on a screw-driven testing machine (INSTRON 5566) at a nominal displacement rate of 2 mm/min. Three dog-bone samples of the PLA material (see Figure 14 (a)) are fabricated for the test. A camera (Canon) was used to track the strains along the loading direction and the transverse direction, and the applied load was obtained by the load cell of the test machine. The typical stress-strain curves of the samples are shown in Figure 14 (c). A fractured sample is shown in Figure 14 (b). It can be found that three stress–strain curves exhibit the near linearity at small deformations (lower than 4%). The experimental results show that the Young's modulus and the Poisson's ratio of the PLA material are E=1210 MPa and ν=0.4, respectively.

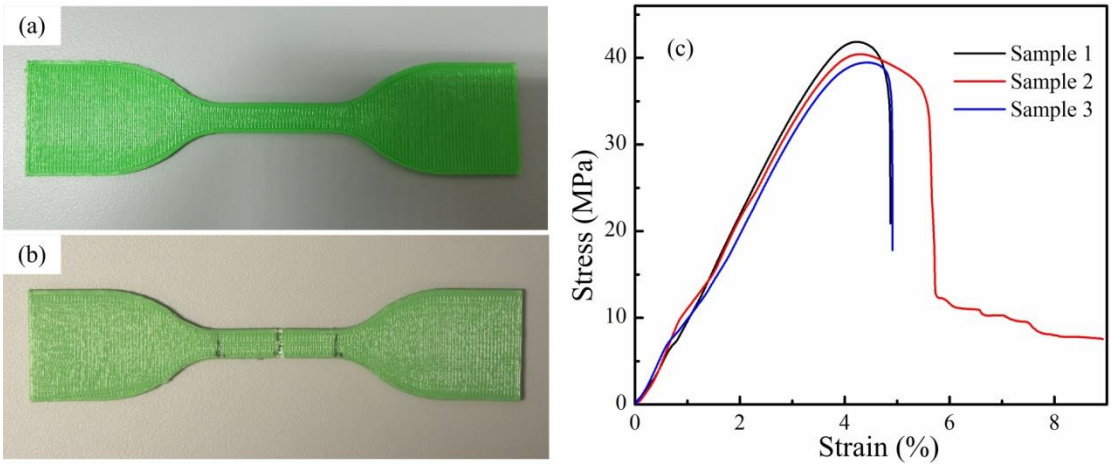

Figure 14. The dog-bone sample (a) before the fracture and (b) after the fracture, and (c) the stress-strain curves under the uniaxial tension test.

The elastic mechanical properties of the hybrid structure are evaluated by the uniaxial compression tests. The hybrid structure samples (see Figure 15 (a) and (b)) are also

fabricated by the 3D printing technology. To reduce the influence of any boundary effects, all of the samples consist of at least 3 unit cells in the vertical and horizontal directions. The geometric parameters of the hybrid structure samples are designed with l_{s1}=l_{s2}=20 mm, and t_0=t_1=t_2=2 mm. Two types of the hybrid structures are fabricated with different θ_2 (60° and 70°). Each type of the hybrid structure has three samples to ensure the repeatability of the experimental results. The compression tests are conducted along the vertical direction and horizontal direction of each sample, respectively, as shown in Figure 15 (a) and (b). The same INSTRON testing machine was used and a displacement rate of 1 mm/min was set. The compressive stress-strain curves of the hybrid structure samples with θ_2=60° along the vertical and horizontal directions, respectively, as shown in Figure 15 (c) and (d), while those of the samples with θ_2=70°are shown in Figure 15 (e) and (f), respectively. All stress-strain curves exhibit the linear elastic behavior at small deformations (lower than 2%). Since the end surface of the samples in contact with the metal disk of the testing machine is not flat enough, the initial phase of stress-strain curve shows the nonlinear behavior. The experimental results of the Young's modulus in the vertical and horizontal directions are compared with the corresponding theoretical and numerical results, as demonstrated in Figure 16. It can be seen that the experimental results show the reasonable agreement with the theoretical predictions and numerical simulations, which also verifies the reliability of the theoretical and numerical models. The main reason for the errors is that the friction between the hybrid structure sample and the metal disk is not considered in the theoretical and numerical analysis.

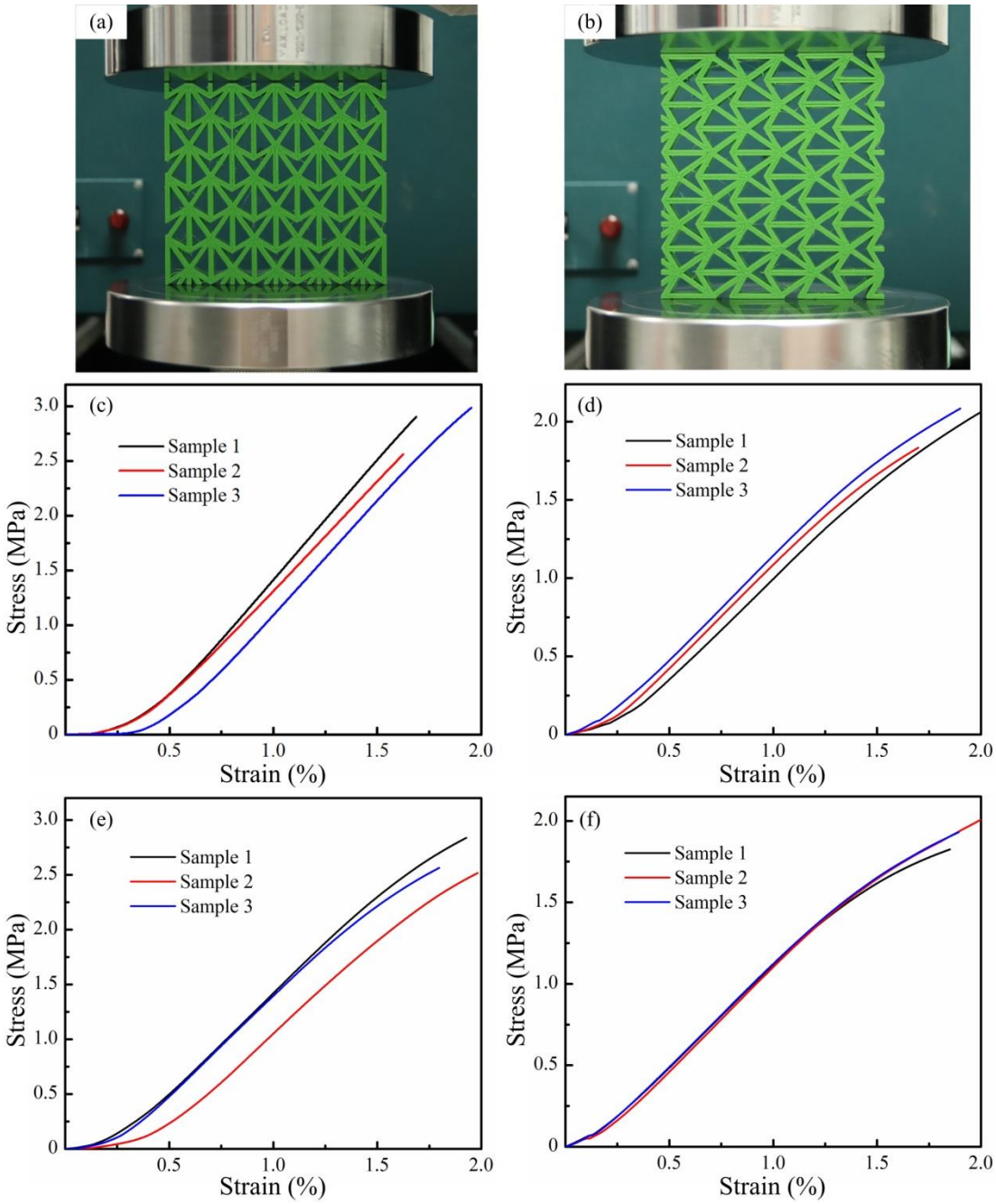

Figure 15. Compressive mechanical behavior of hybrid structures with θ_2=60° and θ_2=70° in the vertical and horizontal directions. (a) Sample loaded along its vertical direction, (b) Sample loaded along its horizontal direction. (c) and (d) the stress-strain curves of samples with θ_2=60°, and (e) and (f) the stress-strain curves of samples with θ_2=70°. (c) and (e) along the vertical direction, (d) and (f) along the horizontal direction.

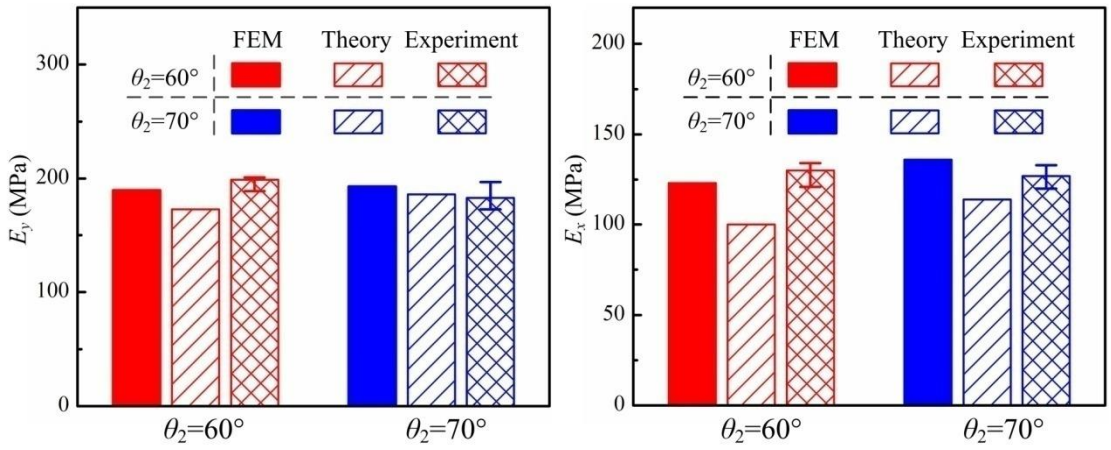

Figure 16. The theoretical, numerical and experimental results of the Young's modulus of the hybrid structures with θ_2=60° and θ_2=70° (a) in the vertical direction and (b) in the horizontal direction.

6 Conclusions

This paper presents a novel mechanical meta-material with enhanced mechanical properties by combining the re-entrant and double-arrowhead structures based on the structural stretching-dominated deformation mechanism. As a new type of hybrid auxetic structure, its unit cell is comprised of the external quadrilateral frame and the internal arrowhead part. Both the theoretical analysis model and FE model are developed to investigate the in-plane mechanical properties in the principal directions. Meanwhile, the elastic mechanical properties of the hybrid auxetic structure made of the PLA material are also analyzed through the experiment. The theoretical predictions show good agreement with the numerical simulations and the experimental measurements. Based on the developed theoretical model, a parametric analysis of the in-plane mechanical properties of the hybrid structure are also performed, including the width of the hybrid auxetic unit cell l_{s2}, the length of the vertical wall l_{s1} and the angle of the inclined wall θ_2 in the internal arrowhead part, and the thickness of the inclined wall t_1 in the external quadrilateral frame. The main conclusions can be summarized as follows. For the hybrid structure when l_{s1}=l_{s2}, simultaneously reducing l_{s1} and l_{s2} can enhance both the Young's modulus in two principle directions, and the variation of the Poisson's ratio with θ_2 exhibits the non-monotonic behavior. Both the NPR behavior and the load-bearing capacity of the hybrid structure in the vertical direction can be enhanced by increasing l_{s1} or reducing θ_2. Increasing l_{s2} can improve the elastic mechanical property in the horizontal direction but reduce that in the vertical direction, indicating that the hybrid structure with the obvious difference of the mechanical properties between the two principle directions can be obtained by adjusting l_{s2}. Increasing t_1 can enhance the mechanical properties but weaken the NPR behavior in two principle directions. Compared with the traditional re-entrant structure, the hybrid structure demonstrates the better elastic mechanical properties and a wider and tunable range of Poisson's ratio from negative to positive. The present work can provide a guidance for the design and fabrication of the hybrid auxetic structures for the practical applications.

Acknowledgements

The authors would like to thank the funding support from the Research Grants Council of Hong Kong Special Administrative Region Government for the NSFC/RGC Joint Research Scheme (Grant number: N_PolyU516/20 and No.12061160461).

References

[1] Lakes R . Foam structures with a negative Poisson's ratio. Science 1987;235:1038–40 .

[2] Alderson K , Fitzgerald A , Evans K . The strain dependent indentation resilience of auxetic microporous polyethylene. J Mater Sci 2000;35:4039–47 .

[3] Choi J , Lakes R . Fracture toughness of re-entrant foam materials with a negativePoisson's ratio: experiment and analysis. Int J Fract 1996;80:73–83.

[4] Scarpa F , Ciffo L , Yates J . Dynamic properties of high structural integrity auxetic open cell foam. Smart Mater Struct 2004;13:49–56 .

[5] Alderson A , Rasburn J , Evans K . Mass transport properties of auxetic (negative Poisson's ratio) foams. Phys Status Solidi b 2007;244:817–27 .

[6] Evans K. The design of doubly curved sandwich panels with honeycomb cores. Compos Struct 1991;17:95–111 .

[7] Ren, Xin, et al. Auxetic metamaterials and structures: a review. *Smart materials and structures*, 2018, 27.2: 023001.

[8] Ferreira, Rafael Thiago Luiz, et al. Experimental characterization and micrography of 3D printed PLA and PLA reinforced with short carbon fibers. *Composites Part B: Engineering*, 2017, 124: 88-100.

[9] Wang, Zhenwei, et al. Progress in auxetic mechanical metamaterials: structures, characteristics, manufacturing methods, and applications. *Advanced Engineering Materials*, 2020, 22.10: 2000312.

[10] Lakes R, Elms K. Indentability of conventional and negative Poisson's ratio foams. Journal of Composite Materials. 1993;27(12);1193-1202

[11] Zadpoor, Amir A. Mechanical meta-materials. *Materials Horizons*, 2016, 3.5: 371-381.

[12] Wu, Wenwang, et al. Mechanical design and multifunctional applications of chiral mechanical metamaterials: A review. *Materials & Design*, 2019, 180: 107950.

[13] Grima, Joseph N.; Alderson, Andrew; Evans, K. E. Auxetic behaviour from rotating rigid units. Physica status solidi (b), 2005, 242.3: 561-575.

[14] Ai, L.; Gao, X.-L. Three-dimensional metamaterials with a negative Poisson's ratio and a non-positive coefficient of thermal expansion. *International Journal of Mechanical Sciences*, 2018, 135: 101-113.

[15] PARK, Jung Jae; WON, Phillip; KO, Seung Hwan. A review on hierarchical origami and kirigami structure for engineering applications. *International Journal of Precision Engineering and Manufacturing-Green Technology*, 2019, 6.1: 147-161.

[16] TANG, Yichao; YIN, Jie. Design of cut unit geometry in hierarchical kirigami-based auxetic metamaterials for high stretchability and compressibility. *Extreme Mechanics Letters*, 2017, 12: 77-85.

[17] LIU, Wangyu, et al. In-plane dynamic crushing of re-entrant auxetic cellular structure. *Materials & Design*, 2016, 100: 84-91.

[18] CHEN, Ganchao, et al. Design and modelling of auxetic double arrowhead honeycomb core sandwich panels for performance improvement under air blast loading. *Journal of Sandwich Structures & Materials*, 2020, 1099636220935563.
[19] Liu Q, Ma J, He Z, Hu Z, Hui D. Energy absorption of bio-inspired multi-cell CFRP and aluminum square tubes. Compos Part B 2017; 121:134-144.
[20] Zou M, Xu S, Wei C, Wang H, Liu Z. A bionic method for the crashworthiness design of thin-walled structures inspired by bamboo. Thin Wall Struct 2016;101:222-230.
[21] Huang H, Xu S. Crashworthiness analysis and bionic design of multi-cell tubes under axial and oblique impact loads. Thin Wall Struct 2019; 144:106333
[22] JIANG, Hongyong, et al. Crashworthiness of novel concentric auxetic reentrant honeycomb with negative Poisson's ratio biologically inspired by coconut palm. *Thin-Walled Structures*, 2020, 154: 106911.
[23] ZHANG, Xin-chun, et al. Dynamic crushing responses of bio-inspired re-entrant auxetic honeycombs under in-plane impact loading. *Materials Today Communications*, 2020, 23: 100918.
[24] WANG, Fengwen. Systematic design of 3D auxetic lattice materials with programmable Poisson's ratio for finite strains. *Journal of the Mechanics and Physics of Solids*, 2018, 114: 303-318.
[25] Radman A, Huang X, Xie YM. Topological optimization for the design of icrostructures of isotropic cellular materials. Eng Optim 2013;45:1331–48.
[26] ZHENG, Yongfeng, et al. Evolutionary topology optimization for mechanical metamaterials with auxetic property. *International Journal of Mechanical Sciences*, 2020, 179: 105638.
[27] KAMINAKIS, Nikolaos T.; STAVROULAKIS, Georgios E. Topology optimization for compliant mechanisms, using evolutionary-hybrid algorithms and application to the design of auxetic materials. *Composites Part B: Engineering*, 2012, 43.6: 2655-2668.
[28] Nguyen, Chuong, et al. Three-dimensional topology optimization of auxetic metamaterial using isogeometric analysis and model order reduction. *Computer Methods in Applied Mechanics and Engineering*, 2020, 371: 113306.
[29] Yang, Hang; Wang, Bing; Ma, Li. Designing hierarchical metamaterials by topology analysis with tailored Poisson's ratio and Young's modulus. *Composite Structures*, 2019, 214: 359-378.
[30] Zhang, Huikai; Luo, Yangjun; Kang, Zhan. Bi-material microstructural design of chiral auxetic metamaterials using topology optimization. *Composite Structures*, 2018, 195: 232-248.
[31] Xu M, Xu Z, Zhang Z, Lei H, Bai Y, Fang D. Mechanical properties and energy absorption capability of AuxHex structure under in-plane compression: heoretical and experimental studies. Int J Mech Sci 2019;159:43–57.
[32] ALI, Md Hazrat; BATAI, Sagidolla; KARIM, Dulat. Material minimization in 3D printing with novel hybrid cellular structures. *Materials Today: Proceedings*, 2021, 42: 1800-1809.
[33] Guo M-F, Yang H, Ma L. Design and characterization of 3D AuxHex lattice tructures. Int J Mech Sci 2020;181:105700
[34] ZHANG, Wenjiao, et al. In-plane mechanical behavior of novel auxetic hybrid metamaterials. *Thin-Walled Structures*, 2021, 159: 107191.
[35] GAO, Ying, et al. New concept of carbon fiber reinforced composite 3D auxetic lattice structures based on stretching-dominated cells. *Mechanics of Materials*, 2021, 152: 103661.
[36] QI, Chang, et al. Quasi-static crushing behavior of novel re-entrant circular auxetic

honeycombs. *Composites Part B: Engineering*, 2020, 197: 108117.

[37] LV, Weitao; LI, Dong; DONG, Liang. Study on mechanical properties of a hierarchical octet-truss structure. *Composite Structures*, 2020, 249: 112640.

[38] LOGAKANNAN, Krishna Prasath, et al. Quasi-static and dynamic compression behaviors of a novel auxetic structure. *Composite Structures*, 2020, 254: 112853.

[39] GUO, Meng-Fu; YANG, Hang; MA, Li. Design and analysis of 2D double-U auxetic honeycombs. *Thin-Walled Structures*, 2020, 155: 106915.

[40] ZHANG, Wenjiao, et al. In-plane mechanical behavior of a new star-re-entrant hierarchical metamaterial. *Polymers*, 2019, 11.7: 1132.

[41] DESHPANDE, V. S.; ASHBY, M. F.; FLECK, N. A. Foam topology: bending versus stretching dominated architectures. *Acta materialia*, 2001, 49.6: 1035-1040.

[42] Gao Y, Wu Q, Wei X, Zhou Z, Xiong J. Composite tree-like re-entrant structure with high stiffness and controllable elastic anisotropy. International Journal of Solids and Structures. 2020;206:170-82.

[43] MAXWELL, J. Clerk. L. on the calculation of the equilibrium and stiffness of frames. *The London, Edinburgh, and Dublin Philosophical Magazine and Journal of Science*, 1864, 27.182: 294-299.